Combustion and Flame 200 (2019) 23–31

Contents lists available at ScienceDirect

Combustion and Flame

journal homepage: www.elsevier.com/locate/combustflame

Particle formation in premixed ethylene-benzene flames: An experimental and modeling study

Mariano Sirignano[a,*], Anna Ciajolo[b], Andrea D'Anna[a], Carmela Russo[b]

[a] Dipartimento di Ingegneria Chimica, dei Materiali e della Produzione Industriale - Università, degli Studi di Napoli Federico II, P.le Tecchio 80, 80125 Napoli, Italy

[b] Istituto di Ricerche sulla Combustione, Consiglio Nazionale delle Ricerche, P.le Tecchio 80, 80125 Napoli, Italy

ARTICLE INFO

Article history:
Received 28 July 2018
Revised 3 October 2018
Accepted 9 November 2018
Available online 22 November 2018

Keywords:
Soot
Premixed flames
Fuel aromatic effect
Benzene
Modeling
Diagnostics

ABSTRACT

In this work soot formation was studied in laminar premixed flames of binary ethylene-benzene mixtures varying throughout the composition range from pure ethylene to pure benzene keeping constant the equivalence ratio ($\varphi = 2$) and obtaining a very similar maximum temperature (Tmax around 1750 K). In such way, it was possible to study for the first time the effect of binary aliphatic-aromatic fuel mixtures composition on the sooting behavior in comparable combustion conditions. In-situ optical techniques (laser induced incandescence and fluorescence) and ex-situ particle size distribution (PSD) measured downstream of the flame front, as well as modeling by means of a multi-sectional method, were applied. PSD profiles showed that particles with sizes less than 10 nm decrease as benzene percentage in the feed mixture increases, disappearing for benzene percentages above 30%. Conversely, large aggregates grow towards sizes larger than 100 nm when benzene concentration is increased. A non-linear effect of the benzene content in the binary fuel mixture on soot particle concentration was observed by laser induced incandescence, and confirmed by the multi-sectional model. In particular soot formation was found to increase more than linear up to 50% then leveled off to reincrease linearly from 80% to 100%. On the contrary, particles smaller than 10 nm at the end of the flame rapidly decreased for benzene percentages larger than 30%. From reaction rate analysis, the formation of gas-phase polycyclic aromatic hydrocarbons (PAH) and high-molecular mass aromatics precursors was found to be significantly large already for fuel mixtures featured by low benzene amounts (from 10 up to 40–50%). The enhanced aromatic precursor formation, combined with the abundance of acetylene mainly coming from the dehydrogenation of ethylene as predominant component of the binary fuel mixture, appeared to be responsible for the non-linear effect of ethylene-benzene composition on particle formation, particularly significant up to 40–50% of benzene.

This finding has a considerable importance as regards the exploitation of highly-aromatic fuels as well as to foresee the soot emission for effect of the aromatic presence in natural and synthetic fuels used in practical combustion systems.

1. Introduction

Soot formation in practical combustion systems is still a major concern, in particular for combustion devices where it is not feasible to apply after-treatment systems to control soot emission. The improvement of combustion efficiency along with the use of "cleaner" fuels as biofuels [1] and fuels with reduced contents of highly-sooting hydrocarbon components [2] has been the approach pursued to reduce soot formation and consequent emission. Surrogate fuels including aromatic components up to 20–30% have been designed to mimic the combustion behavior of real fuels in order to increase the knowledge of their behaviors necessary for improving combustion efficiency and reducing pollutant emissions [3–7]. Indeed, fuel molecular structure plays an important role in the formation and growth of both high molecular weight compounds as polycyclic aromatic hydrocarbons (PAH) and soot [8,9]. The reduction of aromatic components in new formulated fuels is often considered strategic in soot reduction in practical combustion systems [10].

* Corresponding author.
E-mail address: mariano.sirignano@unina.it (M. Sirignano).

https://doi.org/10.1016/j.combustflame.2018.11.006

Table 1
Temperature maximum values and relative flame locations of the ethylene-benzene flames ($\varphi = 2$, carbon flow rate = 16.5 mg/s, cold gas velocity = 4 cm/s@STP).

%Benzene as $C_{Benzene}/C_{total}$	0	5	10	15	20	25	30	40	50	60	80	100
Max temperature, K($\pm$50)	1740	1745	1751	1758	1764	1760	1756	1773	1794	1816	1814	1771
Max temperature position (HAB), mm ($\pm$0.5)	2	2.5	2.5	2.5	2.5	2.5	2.5	2	2	2	2	3

Many experimental and numerical works have been conducted to investigate the role of aromatics on soot formation, but generally, aromatics constitute a dopant in the fuel hydrocarbon mixtures, i.e., their content varies from ppm to few percentages [11].

The chemical structure of premixed flames burning the prototype aromatic hydrocarbon, i.e., benzene, has been previously investigated in terms of gas-phase and condensed phases at low- [12] and atmospheric-pressure conditions [13]. Thereafter, the chemical and morphological characterization of condensed phases, including soot and organic carbon, formed in benzene flames has been carried out in comparison with aliphatic flames [14–19]. Particle size distributions (PSDs) have been measured in premixed flames fueled with pure ethylene and pure benzene at two equivalence ratios [20] showing a not persisting nucleation mode in the benzene flames. PSDs of soot from ethylene flames doped with benzene have been measured [21], however the significant change of the feed velocity, and hence of temperature, in the investigated flames did not allow a direct comparison of PSDs among different conditions. Sooting tendency of aromatic hydrocarbons has been evaluated by measuring maximum soot volume fractions on the centerline of a coflowing methane/air non-premixed flame doped with 400 ppm of selected aromatics [22]. More recently, the study of the effect of alkyl-substituted aromatics on soot formation has been studied in opposed flow flames with aromatic hydrocarbons being fed up to 30% [23]. The study of the effect of n-propylbenzene addition to n-dodecane on soot formation and aggregate structure in a methane laminar coflow diffusion flame [24] showed that aromatic fuel chemistry strongly affects soot inception. Toluene added to a premixed methane flame as 10% of the total feed carbon has shown to have a considerable impact on soot formation despite of the small toluene percentage used [25,26]. In sooting laminar premixed flames aromatic addition (10 vol% of n-propylbenzene) to n-heptane fuel has shown an increased and earlier formation of benzene and PAH without significantly changing the final soot loading [27].

Many other studies have been also recently conducted varying the aromatic content and by using reference fuels, however in all these studies the combustion conditions strongly changed for effect of the aromatic addition. For instance, PSDs were measured in burner-stabilized stagnation flames by varying the aromatic content in the heptane/toluene mixture, but the maximum temperature of the investigated flames changed by 150 K and the equivalence ratio varied from 1.89 to 1.69 [28]. In another case [29], the combustion conditions adopted - a wick-fed diffusion flame- did not allow to have well-controlled boundary conditions, and thus to perform reliable modelling for highlighting the different formation pathways.

Experimental findings have been used to predict soot evolution in aromatic-fueled flames [14,20,24,27,30]. In aliphatic-fueled flames the slow conversion of the aliphatic molecule to aromatic compounds is the limiting step for the formation of the first particle and hence of soot. In aromatic flames, this step is overtaken and aromatics are present well deep in the flame front zone, inducing the formation of first particles in the early oxidation stage. Likewise, smaller particles (sizes less than 10 nm) and large aromatic compounds are formed already at the flame front of aromatic flames, before soot inception, and are then rapidly consumed, with the small nanoparticles dropping down to non-detectable concentration levels downstream of the flame front [14]. On the other hand, aliphatic fuels show a persistency of small nanoparticles along with larger particles/aggregates, i.e., a clear bimodality of the particle size distribution at the end of the flames [14].

Actually, the soot yield increase for effect of the addition of even few amounts of aromatics to aliphatic hydrocarbons [e.g. 25,26] casts some doubts about the occurrence of synergistic effects as those already observed in binary mixtures of aliphatic hydrocarbons [31–33]. In this framework, the present study reports for the first time a study of the effect of aromatic fuel content on particle formation in well-controlled conditions of premixed flames at fixed equivalence ratio and keeping rather constant the temperature. In-situ optical techniques and on-line ex-situ scanning mobility particle size (SMPS) analysis of sampled particulate matter have been systematically applied in premixed flames varying the binary ethylene-benzene composition in the whole 0–100% range. Multisectional kinetic model and a reaction analysis have been also used to predict and understand the mechanism of formation of the particulate matter of ethylene-benzene mixtures.

2. Experimental methods

Ethylene/benzene mixtures with varying composition have been fed to a premixed flame capillary burner at atmospheric pressure and fixed equivalence ratio ($\varphi = 2$) corresponding to the visible soot threshold in the pure ethylene flame, and keeping constant the total carbon flow rate (16.5 mg/s) and cold gas velocity (4 cm/s @STP). To keep constant the carbon flow rate and flame temperature at varying mixture compositions, the flames were burned in an oxygen/nitrogen mixture tuning the nitrogen content starting from the pure atmospheric-pressure benzene flame previously studied [13].

Flame temperature profiles were measured using a 250 µm bead-size Type-R thermocouple, applying radiation correction with the methodology developed by Eisner and Rosner [34]. The peak temperature in the flame is strongly affected by the heat exchange between the flame and the burner; the relative low velocity of the cold gas enhances this effect. This peculiar characteristic of the premixed burner, together with the choice of fixing the equivalence ratio ($\varphi = 2$) and the total carbon fed, made the maximum temperature to remain rather constant as varying benzene/ethylene feed mixture despite the change of the heat of combustion of the binary mixtures.

A slight variation of the maximum peak temperature values and flame front locations, measured for the investigated flames and shown in Table 1, can be noticed. These differences do not follow a specific trend with the benzene content. If a mean temperature is considered (1770 K), a standard deviation of 25 K (1.5%) can be evaluated, mostly coming from the inherent thermocouple error and flame fluctuations. The maximum flame temperature is strongly determined by the heat exchange with the burner in our experimental apparatus. Moreover, the similarity of the overall heat release of the flames and the very low cold gas velocity (4 cm/s) determine a small change in the maximum flame temperature. The measured temperature profiles (not reported) are also similar with a decrease downstream of the flame as the soot volume fraction increases. The differences at the end of the flame

where the soot volume fraction maximizes are contained within 100 K between pure benzene and pure ethylene flame. It is worth to remind that the measurements at the end of the flame are affected by soot deposition. However, there is no soot deposition at the flame front where soot is not present. Hence, the temperature measurements at the peak are not affected by this phenomenon.

LIE (Laser Induced Emission) measurements were performed by an ultrafast gated ICCD in the 200–550 nm range, using as excitation source the fourth harmonic of a Nd:YAG laser at 266 nm with a fluence of 0.8 J/cm^2 using the same experimental setup used in previous works [35–38]. In a previous paper [38] we have shown that, under UV laser pulse excitation, small size, sub-10 nm, particles, formed in premixed flames show broadband fluorescence signals from UV to the visible (Laser Induced Fluorescence - LIF) whereas larger particles incandesce after heating-up (Laser Induced Incandescence - LII). Also in the present work, carried out in the same conditions of [38] - laser pulse at 266 nm, spectral acquisition, ultrafast gated camera - the main contribution to the LIF signal is attributed to so-called condensed phase nanostructures (CNP). LIF from PAHs has been evaluated as marginal although possible, due to their very low quantum yield at the investigated conditions (very low decay time) with respect to very high quantum yield coming from CNP (long decay time of LIF signal).

The size of the smallest particle able to be reliably detected by LII is a current topic for the community [39–41]. However, the LII signal is generally proportional to the particle volume fraction and thus more sensitive to the largest particles present in the combustion environment. In case of a bimodal particle size distribution, with the simultaneous presence of large aggregates - up to 100 nm and more - and small primary particles - down to few nanometers - LII will track the total volume fraction and thus the concentration of large aggregates. More details about the LII technique used also in this work, and its validation against other optical techniques and ex situ analysis are reported in ref [38].

In order to retrieve the particle size distributions (PSDs), particulate matter has been sampled by a stainless steel probe placed horizontally at a different height above the burner (HAB), namely from 6 to 15 mm, and classified by scanning mobility particle sizer (SMPS) analyzer. In the present work, the probe has an ID = 8 mm, a wall thickness of 0.5 mm, and a pinhole diameter of 0.8 mm [38, 42-44]. This large pinhole can cause a large perturbation of the probe; however, the measurement have been compared with a satisfying agreement with the small pinhole [43]. A two-stage dilution system has been used: the carrier gas - nitrogen - has been set to 4 l/min (at 273 K) for the first dilution and to 65 l/min in the second dilution stage. An overall dilution of 500 is achieved for the investigated conditions with a global residence time in the probing systems of 100 ms before entering in the detection system.

For the PSD measurements, a nano-DMA has been used (TapCon 3/150 DMA system in high voltage mode corresponding to a nominal size range 2–100 nm equipped with a Faraday Cup Electrometer detector). At the entrance of the DMA, particles were taken to Fuchs' steady-state charge distribution [45] by using Soft X-Ray Advanced Aerosol Neutralizer (TSI model 3088). Particles then enter the nano-DMA where they are separated according to their electrical mobility in an electrical classifier. The classified particles are then counted by an Electrometer Faraday Cup. By varying the electrical field applied to separate particles it is possible to rebuild the original PSD. The experimental setup used for PSD determination was accurately developed during the years: it is able to reduce the residence time within the sampling line and, because of a two-stage dilution, it is able to minimize losses as particle coagulation. However, we cannot exclude that small particles might be lost during sampling and the number concentration of very small particles be affected by particle lost, however the differences – in particular the reduction – in small particles concentration by using different percentages of benzene are large, consistent and progressive, indicating the overall reliability of the measurements, at least in the trends presented. The PSDs obtained by DMA were successively corrected for losses in the pinhole and the probe following the procedure reported in the literature [46–48]. DMA separates particles on the basis of their mobility diameter so that finally the particle diameter was retrieved from the correlation proposed by Singh et al. [49].

3. Modeling approach

A multi-sectional kinetic model has been used to predict particle formation of the binary mixtures. The model has been previously tested in aliphatic and aromatic flames in both premixed and diffusion configuration [14,26,50,51] showing good capability to predict soot and condensed phase nanostructures, and in general to predict the evolution of PSD. The model contains a gas phase mechanism that takes into account fuel oxidation and PAH formation and growth, and reactions responsible for particle nucleation. Compounds with molecular weight larger than pyrene are not treated punctually due to the large number of species and of their isomers. The approach to follow the formation of high-molecular weight species is to divide molecules larger than pyrene in intervals of molecular masses and to evaluate a collision frequency and to assign an activation energy for each chemical reaction, i.e., molecular decomposition and growth, H-atom abstraction and oxidation. The molecular mass distribution is defined by a range of sections, each containing a nominal hydrocarbon species in order of increasing atomic mass. Carbon number ranged from 24 to 2x10^{10} and H/C for each carbon number ranges from 0 to 1 covering an equivalent size range of 1–800 nm [52]. Thirty-one sections are used in a geometric series of carbon number with a ratio of two between sections; five sections were used for H/C variation; radical and neutral molecules were separately grouped. Another discretization, which accounted for the level of agglomeration of the compounds, is also introduced; three entities are defined: Molecules, Clusters of molecules or Particles and Agglomerates of particles. Overall, 465 lumped species for the stable form and 465 for radicals are modeled; details of the model are reported elsewhere [53].

A brief description of the most important steps in molecular growth process and particle inception is reported here to help following the discussion, especially on the reaction analysis. Starting from pyrene, the molecular growth of aromatics is initiated by an H atom loss from aromatic molecules or by the spontaneous decomposition of aromatic molecules forming an aromatic radical. Termination reactions of aromatic radicals with other aromatic radicals ended the growth sequence. The formation of PAH molecules is modeled by addition of acetylene, following the HACA sequence. PAH having the lowest amount of H atoms are pericondensed PAH; their H/C ratio decreases to very low values as the molecular size increases. The formation of aromatics connected by σ-bonds, also called σ-dimers, is modeled both by aromatic radical combination and by aromatic radical addition to non-aromatic double bounds. The H/C ratio of the σ-dimers remains comparable to those of the aromatic molecules involved in the reactions and it slowly decreases as the molecular weight of the molecules increases. Both classes of aromatics could grow indefinitely forming extremely large molecules. Together with the chemical growth, the physical process of PAH coagulation, that is long-range interaction between colliding entities, occurred to form clusters of molecules, i.e., first particles. Molecule coagulation is considered irreversible at this stage and its reaction rate is modeled by considering a coagulation efficiency with respect to the collision frequency. More recently, a direct and reverse rate for coagulation of PAH to form clusters and PAH onto existing particles have been

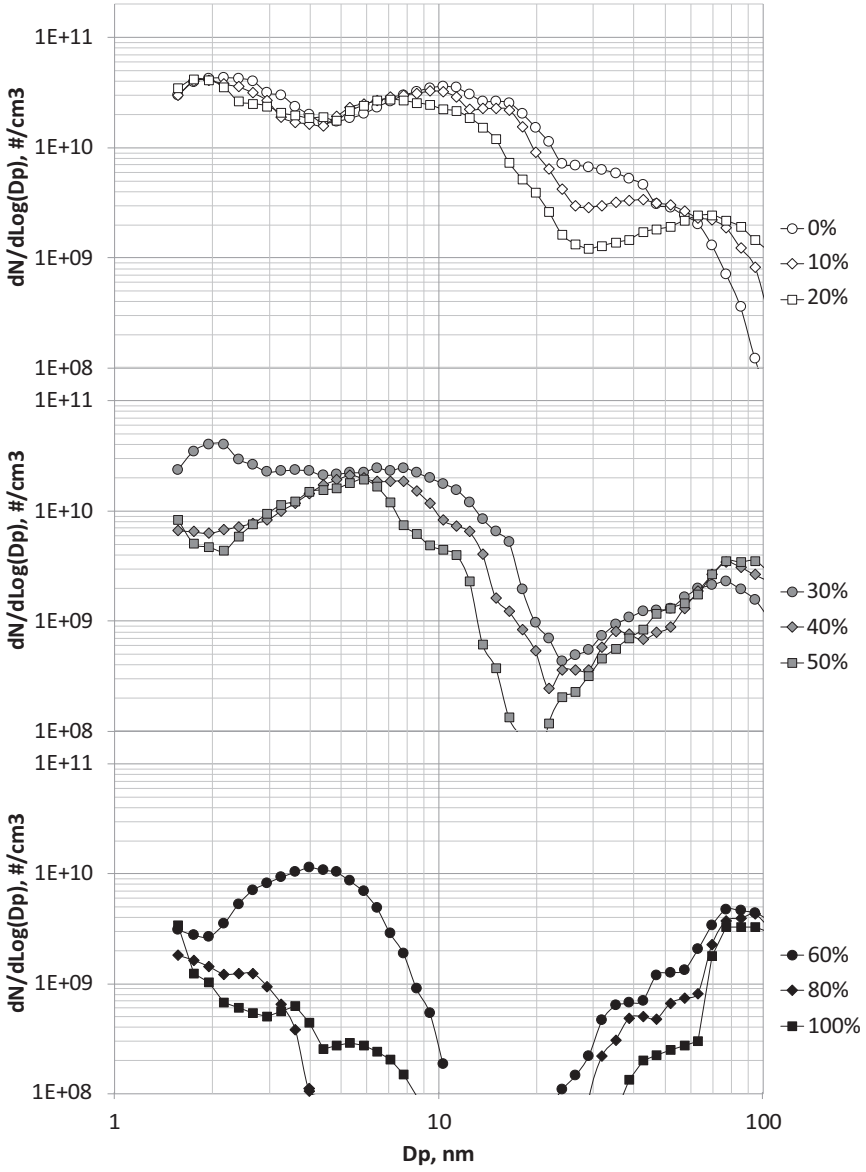

Fig. 1. PSD profiles measured at HAB = 15 mm of the benzene/ethylene flames as a function of benzene content (CBenzene/Ctotal percentage) in the ethylene/benzene fed mixture.

proposed [54]. This approach considers the single reaction rates - forward and reverse - instead of using coagulation efficiency. The collision frequency increases with the increase of molecular mass of the molecules whereas the coagulation efficiency depends on both the temperature and chemical characteristics of the colliding molecules. The chemistry of the particles is considered by evaluating the Hamaker constant [55] for the species involved in the coagulation process. The Hamaker constant accounts for van der Waals body-body interactions. From benzenic ring to graphite the Hamaker constant ranges from $3 \times 1E{-}20$ J to $5 \times 1E{-}19$ J. A value of $5 \times 1E{-}20$ J has been assigned to a compound with an H/C ratio of 0.5. The values of the Hamaker constant for the other compounds have been linearly scaled on the H/C ratio. The coagulation efficiency was evaluated following D'Alessio et al. [56]. The computed coagulation efficiency, of the order of 1E-4 for small colliding entities, increases to values of about 1 when the C number is about 1E6. These values are in agreement with experimental coagulation rates [42,56]

Clusters of molecules (or Particles), constituting the particle nuclei, can continue to react in the same way as the molecules; they can add molecules to increase their size, or remove H-atoms by dehydrogenation or C-atoms by OH and O_2 oxidation, or they can coagulate with other molecules or other clusters. If two clusters merge into one reducing free surface area so as to minimize their free energy, a coalescence event occurs. The formed cluster assumes a spherical shape and can be seen as a cluster of molecules larger than the previous two. As the cluster size increases, the timescale of molecular coalescence becomes larger than the timescale of the agglomeration process and consequently the coagulation events lead to the formation of agglomerates. It appears that particles with an nC of 1×10^5 (equivalent size of about 10 nm) have a rate of coalescence higher than that of agglomeration. This behavior is reversed for structures with nC larger than 1×10^6 (equivalent size of about 20 nm). For particles of 10–20 nm, coalescence and agglomeration rates are similar which means that these particles can coalesce or agglomerate with the same probability. Sensitivity analyses have been conducted by changing the size and H/C ratio dependence of the coalescence rate. The coalescence-agglomeration ratio does not drastically affect the final concentration of the particles but it does determine

the size of the primary particles, which constitutes particle agglomerates. The measured temperatures have been used as input to the model as done in the past for modeling similar flames [26]. The model also indicates that the small variation in the maximum temperatures – within the measurement error – does not give significant changes in the results for soot volume fraction and in the reaction analysis.

4. Results and discussion

The differences in the size of the CPN and soot generated by the ethylene-benzene mixtures can be seen in Fig. 1 reporting the PSDs measured downstream of the different ethylene-benzene flames (HAB = 15 mm).

The PSD of the pure ethylene flame shows a tri-modal size distribution:

- the first mode includes particles in the range 1–5 nm defined CPN and showing LIF signals from UV to visible [38],
- the second mode, up to about 30 nm, is constituted of primary soot particles that are able to incandesce upon laser irradiation,
- the third mode includes aggregates of primary particles with sizes up to about 100 nm in the pure ethylene flame, also able to incandesce.

By adding up to about 20–30% of benzene, the PSD shape does not significantly change showing only the second mode slightly shifting towards smaller particles and the third one extending much above the detection limit of 100 nm.

Above 30% of benzene, the amount of small particles belonging to the first mode is strongly reduced (more than one order of magnitude) and even the amount of the second mode particles decreases in favor of particle aggregates with sizes much larger than 100 nm, thereby indicating the occurrence of a strong agglomeration. The presence of a significant number of particles larger than 100 nm, out of the available range of measurements, did not allow retrieving a reliable value of the volume fraction from the PSD.

Above 50% of benzene, the PSD becomes bimodal and especially for 80% and 100% benzene flames, the number concentration of the small particles falls below the detection limit and only very large soot aggregates are formed. The "scavenger" effect of large aggregates on small particles both in the flame and in the sampling line cannot be excluded even in presence of an adequate dilution.

The LIF and LII signals, associated to the CPN and soot primary and aggregate particles, respectively, are in agreement with the PSD trends above described (Fig. 1), as illustrated in Fig. 2 reporting LIF and LII signals for selected benzene percentages (0%, 20%, and 100%). LIF signal detected at 350 nm (LIF@350 nm) (Fig. 2(a)) evidences the sharp rise-decay profile in the benzene flame different from the LIF profile measured in the ethylene flame that instead slowly decreases after the maximum, attaining to much higher values downstream of the flame. The flame with the 20% of benzene exhibits an intermediate behavior, already evidencing a significant LIF reduction at the end of the flame.

Large differences between benzene and ethylene flames are also evident both in terms of intensity and shape of the LII profiles (Fig. 2(b)). Specifically, the benzene flame exhibits a steep rise of the LII signal, significant of a very rapid soot formation in the first part of the flame, followed by a leveling off to a quite higher value. The ethylene flame presents a lower and much delayed LII signal with respect to the benzene flame slowly increasing along the flame without reaching a plateau. As observed for the LIF signal, already in the 20% benzene flame the LII profile changes in shape – and in this case remarkably increases in the final intensity value – indicating a strong effect of the aromatic presence in fuel mixture on particle formation.

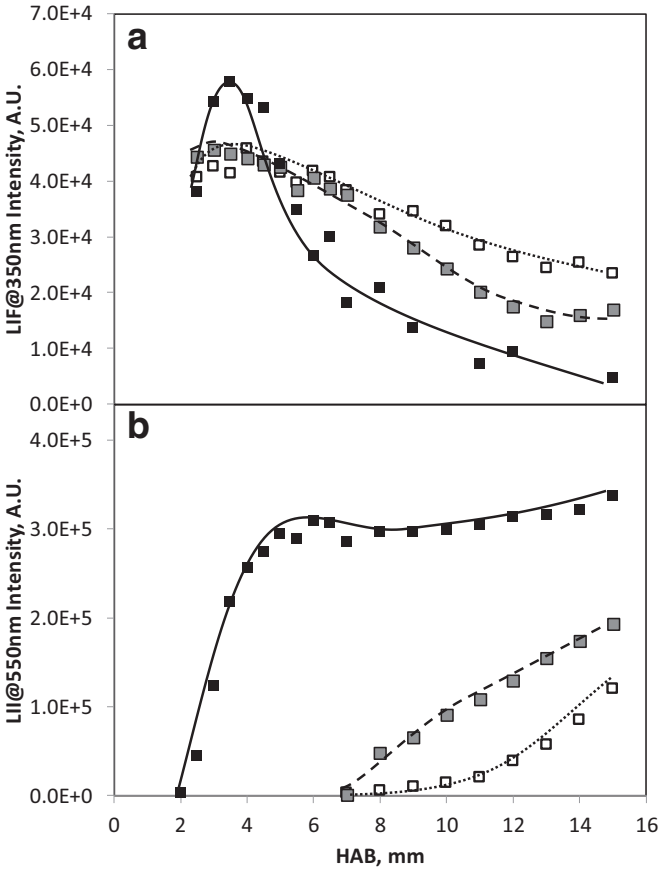

Fig. 2. Axial profiles of LIF (a) and LII (b) signals measured by excitation at 266 nm and detection at 350 and 550 nm, respectively, in neat ethylene (white squares), 20% benzene (grey squares) and 100% benzene flames (black squares). Lines are reported as guidelines.

Overall, the optical measurements and the PSDs reported so far are in good qualitative agreement. A comparison between the volume fraction (or the soot yield) evaluated by optical technique and by PSD is not reported due to the uncertainty in the evaluation from PSD. The main uncertainty is coming from the error in the measured dilution factor. Also, it is not possible to know a priori the fractal size to retrieve the volume fraction from the aggregate mobility diameter. However, the focus of the paper is not a cross validation of the quantification of the soot volume fraction from LII and PSD. Finally, the volume fraction would be correctly evaluated just for the pure ethylene flame. In fact, for the other flames there is a significant number of aggregates outside of the range of detection which constitute part– if not the totality - of the volume fraction.

To track the effect of benzene on total soot formation, Fig. 3 reports the LII signal intensity as a function of the benzene percentage in the fed hydrocarbon mixture. The increase of the LII signal as benzene percentage increases is clearly not linear up to a percentage of almost 60%; the effect is stronger in the range of benzene percentages up to 30% and levels-off to linearity between 30 and 60% of benzene.

Figure 3 reports also the modeled soot yields at the end of the flame (HAB = 15 mm) as a function of the benzene percentage (continuous line). To allow the comparison with LII data, modeled soot yields - reported on a different scale (on the right) of Fig. 3- account for the sum of all the lumped species with an equivalent size > 10 nm, since species with size < 10 nm can be neglected as not contributing to the total mass. In previous work [14] the same model has been successfully tested to predict the pure ben-

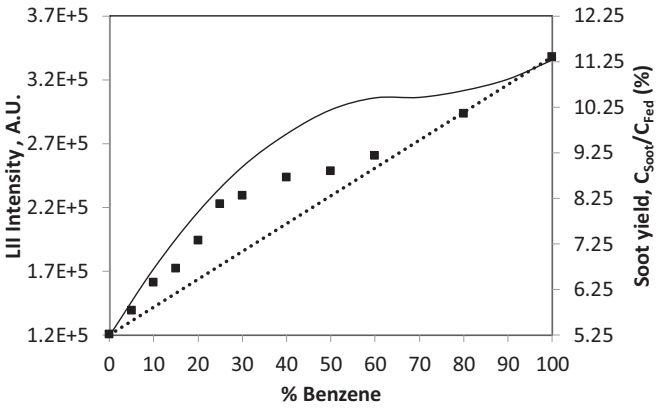

Fig. 3. LII signal (dots, left axis) at HAB = 15 mm vs. benzene percentage. Continuous line (right axis) reports soot yield (%) as predicted by the model. Dotted line is the linear interpolation between the two extremes of mixture composition.

zene flame including soot total amount (measured by gravimetric method), size distribution and H/C ratio. It is important to underline that the model reproduces the non-linear soot yields increase with benzene percentage, without any modification or tuning passing from one mixture condition to another. However, it is remarkable that modeling overrates the benzene enhancement effect between 40% and 80% of benzene content in the fuel. This discrepancy can be due to some overestimation of the contribution of the aromatics to the soot growth as well as to uncertainties on the temperature measurements, especially at the end of the flames, i.e, in very sooting conditions as the high soot loads reduce the temperature of the flame for effect of heat loss by soot radiation.

Model analysis allows retrieving more information on the non-linear effect of benzene percentage on soot formation. The presence of benzene in the fuel mixture implies a high benzene concentration already in the flame front, which helps to overcome the limiting stage of the first aromatic ring formation and causes the consequent increase of PAH production. For small benzene percentages in the fuel mixture, there is a synergistic effect on particle nucleation and loading between the PAH production, coming from benzene consumption pathways, and the acetylene and other small radicals coming from ethylene pathways. As the benzene percentage increases, large PAH formation and nucleation are not enough to compensate for the decreasing concentration of acetylene responsible for soot loading, thereby soot production approaches the linearity. The effect can be understood by the reaction rate analysis summarized in Figs. 4 and 5.

Figure 4 reports the rates (moleC/cm^3 s) of soot production for the different processes involved that are: formation and molecular growth of PAH molecules (panel ***a***), inception of particle/clusters of molecules (panel ***b***), growth by C_2H_2 (panel ***c***) and PAH (panel ***d***) onto existing particles or aggregates. Finally, Fig. 5 reports the ratio between the growth rates by C_2H_2 and PAH.

From a mechanistic point of view, in a flame fueled with an aliphatic, e.g., the pure ethylene flames presented here, benzene is initially formed and then continuously consumed during oxidation, and finally re-formed downstream of the flame front - if enough precursors are available. As net effect, benzene is present at the end of the flame. When benzene is used as fuel, it is oxidized to a large extent and another part is decomposed in smaller fragments. Finally, there is a certain benzene amount that undergoes directly the growth pathways leading to PAH (also but not only passing through the cyclopentadienyl pathway). The reaction

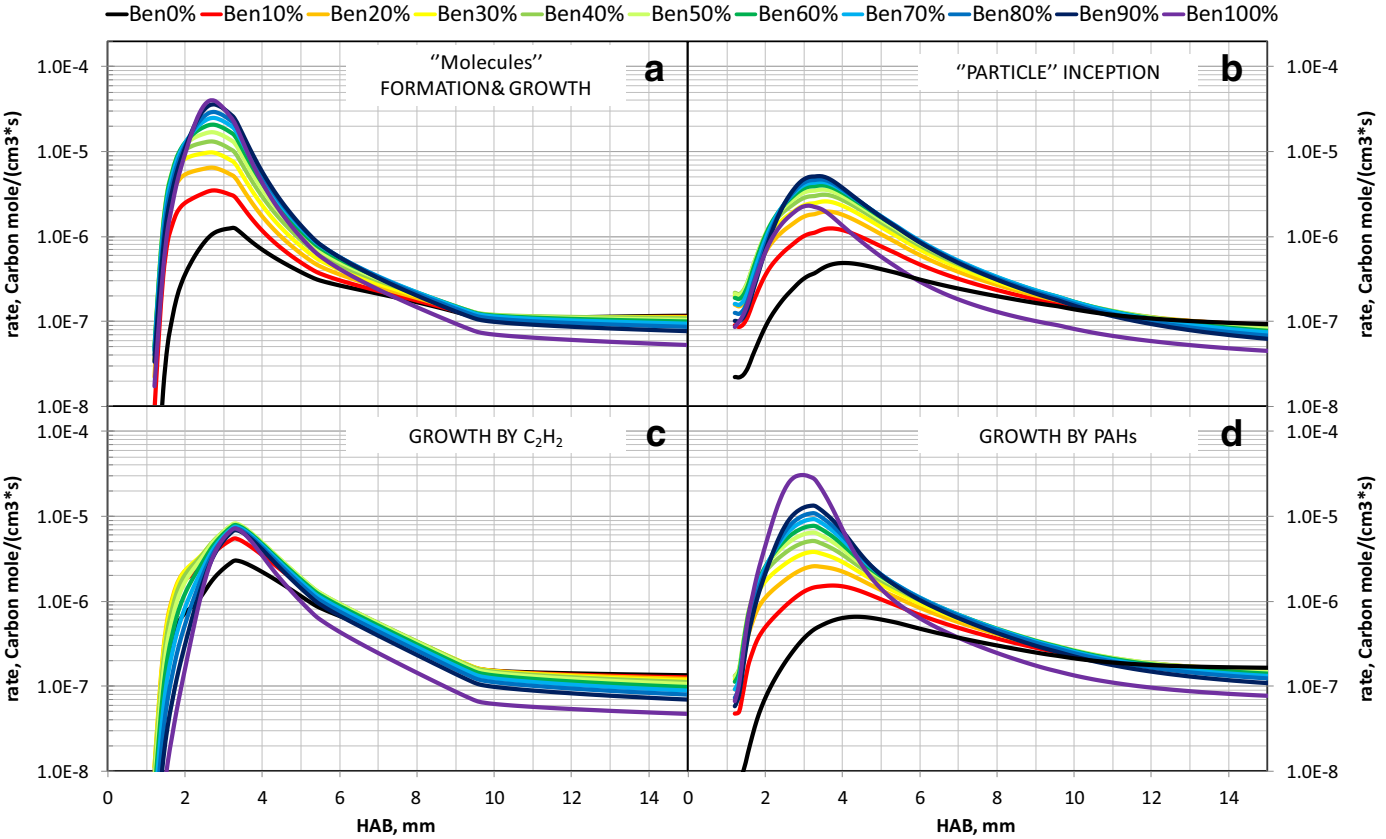

Fig. 4. Modelled reaction rates for different processes: formation and growth of "Molecules" (a), inception of "Particles" (b), growth of "Particles" and "Agglomerates" by C_2H_2 (c) and by PAH (d). Different colors refer to different benzene percentage in the fuel mixture. A color version of the figure is available online.

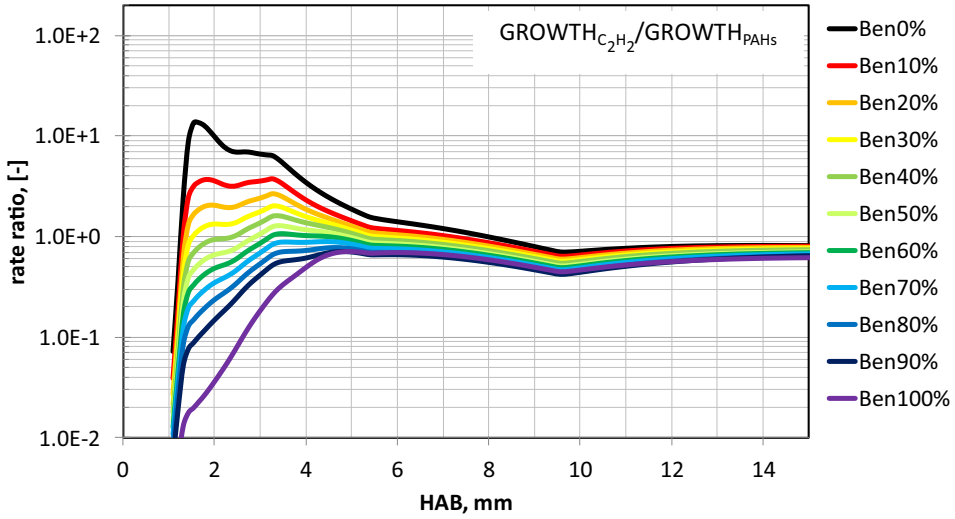

Fig. 5. Ratio between modelled reaction rates of "Particles" and "Agglomerates" growth by C_2H_2 and by PAH. Different colors refer to different benzene percentage in the fuel mixture. A color version of the figure is available online.

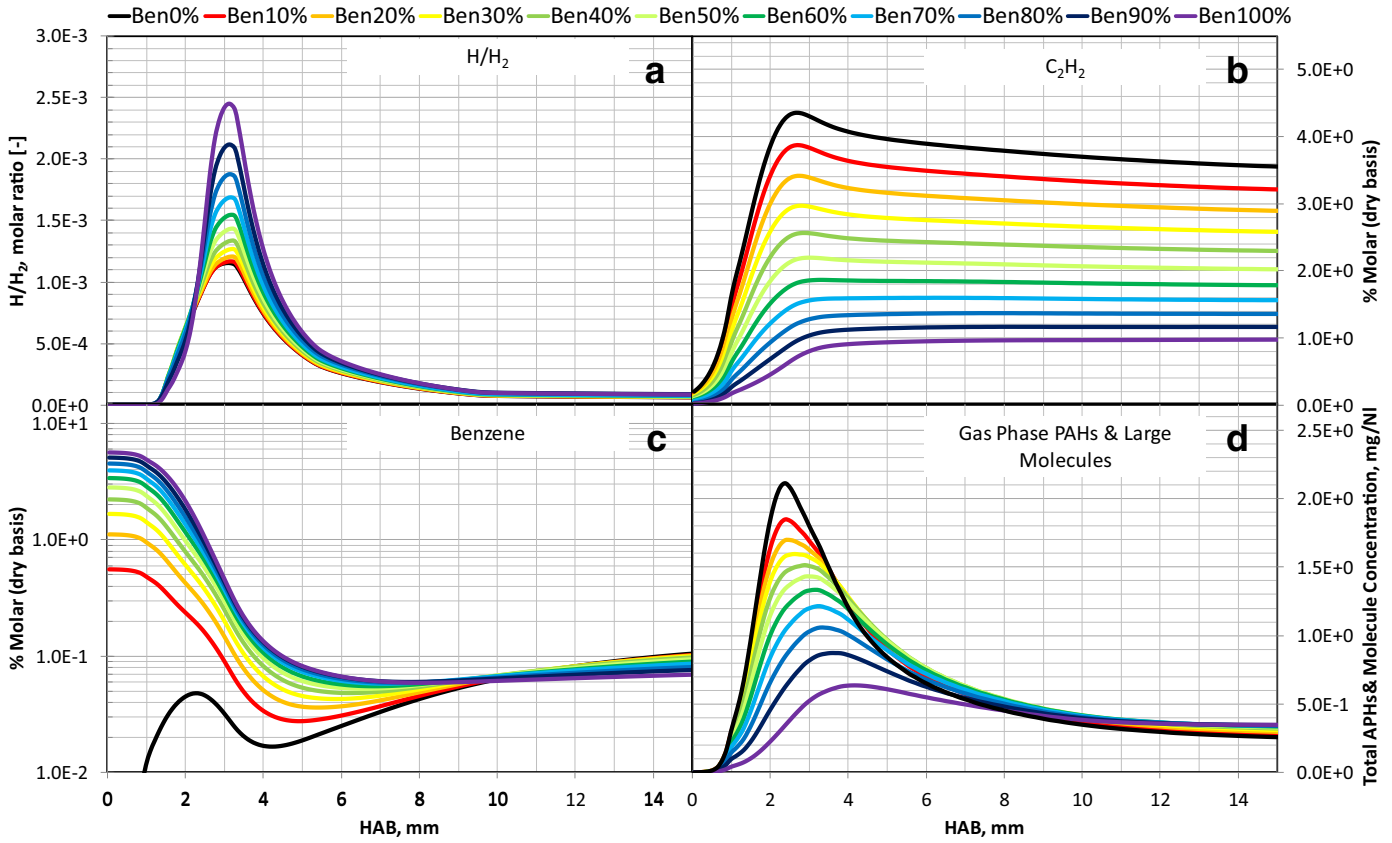

Fig. 6. Modelled concentration for different species: H/H_2 molar ratio (a), C_2H_2 (b), benzene (c) and total gas phase PAH and Molecules (d). Different colors refer to different benzene percentage in the fuel mixture. A color version of the figure is available online.

analysis shows how the synergy between the products from ethylene and benzene mostly regulate the ratio between nucleation/growth pathway.

Modeled data shows how the addition of benzene in the fuel mixture strongly enhances the formation rate of large molecules (Fig. 4, panel ***a***). This behavior is due to the concentration of PAH and large molecules, i.e. high-molecular mass aromatics, increased by the presence of benzene in the mixture and attaining a maximum early in the reaction zone as shown in Fig. 6 where the modeled profiles of H/H2 concentration ratio, acetylene, benzene and aromatic molecules concentration, i.e. total gas phase PAH and Molecules, are reported.

Once gas-phase PAH and large molecules are formed they are able to form clusters, i.e. to "incept" particles (Fig. 4, panel ***b***). The formation of these particles is proportional to aromatics concentration and hence is favored as benzene content in the fuel increases. The earlier formation of these first particles in the flame front where reactivity is high, allows a fast soot growth. However,

C_2H_2 diminishes in concentration as benzene increases as shown in Fig. 6. The net effect is an increase of the growth by C_2H_2 up to 50% of benzene addition and then a decrease for larger amounts of benzene as shown in Fig. 4, panel ***c***. This peculiar behavior is responsible for the non-linear effect of benzene percentage on the total amount of particles. The increase of the growth by acetylene despite of its diminished concentration (Fig. 6, panel ***b***) can be explained by the fact that the benzene addition in the fuel mixture favors the inception of particles due to larger amount of PAH available (Fig. 6- panel ***c***), and higher reactivity as testified by H/H_2 ratio (Fig. 6, panel ***a***); consequently, the simultaneous presence of particles and acetylene allows particles to grow. In other words, the increased inception rate due to the presence of PAH, and consequently all the other large molecules, produces more nuclei for acetylene growth. Hence, the acetylene formed in combustion acts synergically with the benzene present in the fuel mixture and the compounds formed from benzene reactions. The synergic effect for a benzene content in the fuel mixture up to 30% turns into an increased net formation rate; for larger amount of benzene – up to 60–80% - the increase of the inception rate and decrease of acetylene concentration compensate each other levelling off the net formation rate. Eventually, the growth by PAH in pure benzene flame is so enhanced that is even faster than inception - and other processes - and the effect is again an increase of the net formation rate (Fig. 3).

The fast inception and growth by PAH observed close to the flame front when benzene is present in the fuel mixture are responsible for the consumption of all gas-phase PAH, and thus turn into a faster net formation rate in the first part of the flame and in a lower net formation rate at the end of the flame. This peculiarity of the particle formation reflects into the typical sharp soot profile found in the benzene flame and it is responsible for the lack of small particles at the end of the flame as suggested by experimental evidences and confirmed by numerical results. Small particles are able to chemically (by PAH and acetylene addition) and physically (coagulating to form larger particles) grow fast enough because of the higher concentration and the more reactive environment in which they are produced when benzene is fed. At the end of the flame the lack of gas-phase PAH does not allow to have an effective continuous nucleation. On the other side the slower inception and growth rates in the ethylene flame ensure an effective continuous inception that allows to have small particles all along the flame.

5. Conclusions

The effect of benzene fuel content on particle formation was studied in laminar premixed flames of binary ethylene-benzene mixtures, from pure ethylene to pure benzene, by a combination of in situ optical techniques and ex situ PSD measurements as well as the use of multi-sectional method for a deeper interpretation of the experimental results.

Equivalence ratio, $\varphi = 2$, was chosen and kept constant for all the fuel mixture compositions, being on the limit of the visible sooting threshold for the pure ethylene flame. PSDs measured at the end of the flames indicate that the number of particles with sizes less than 10 nm diminishes as benzene percentage in the fuel mixture increases, disappearing for benzene percentages above 30%. Large aggregates on the contrary grow in size reaching sizes larger than 100 nm. A non-linear effect of the benzene percentage on soot particles (detected with LII) was found in the flames. As the benzene percentage increases the flame structure tends toward the structure typical of aromatic hydrocarbon flames with a rapid increase of particle concentration close to the flame front that levels off at the end of the flame. Significant differences with pure ethylene flame are observed already at 20% of benzene in the feed mixture. The condensed phase nanostructures, detected by LIF, follow the same trend with the benzene percentage: as benzene percentage increases the condensed phase nanostructure concentration in the post flame decreases, as typically found in aromatic flames. The model applied to predict particles formation in the investigated flames generally reproduced the non-linear effect of the benzene amount on soot. From the reaction rate analysis, the synergistic effect between the higher formation of gas-phase PAH along with large aromatics, favored by the presence of benzene in the fuel, and the abundance of acetylene, coming mainly from the dehydrogenation of ethylene, comes out to be responsible for the non-linear effect of benzene content in the fed mixture on soot production.

The assessment of the non-linear effect of benzene on soot production in a defined range of benzene content in the fuel mixture has importance as regards the exploitation of heavy highly aromatic fuels as well as of fuels where aromatic addition is used for achieving fuel properties relevant to practical combustion systems.

References

[1] K. Kohse-Höinghaus, P. Oßwald, T.A. Cool, T. Kasper, N. Hansen, F. Qi, C.K. Westbrook, Biofuel combustion chemistry: from ethanol to biodiesel, Angew. Chem. – Int. Ed. 49 (21) (2010) 3572–3597.

[2] H.R Zhang, E.G. Eddings, A.F Sarofim, C.K. Westbrook, Fuel dependence of benzene pathways, Proc. Combust. Inst. 32 (1) (2009) 377–385.

[3] J.M. Simmie, Detailed chemical kinetic models for the combustion of hydrocarbon fuels, Prog. Energy Combust. Sci. 29 (2003) 599–634.

[4] P. Dagaut, M. Cathonnet, The ignition, oxidation, and combustion of kerosene: a review of experimental and kinetic modeling„ Prog. Energy Combust. Sci. 32 (2006) 48–929.

[5] F. Battin-Leclerc, Detailed chemical kinetic models for the low-temperature combustion of hydrocarbons with application to gasoline and diesel fuel surrogates, Prog. Energy Combust. Sci. 34 (2008) 440–498.

[6] W.J. Pitz, C.J. Muller, Detailed chemical kinetic models for the low-temperature combustion of hydrocarbons with application to gasoline and diesel fuel surrogates, Prog. Energy Combust. Sci. 37 (2011) 330–350.

[7] E.G. Eddings, S. Yan, W. Ciro, A.F. Sarofim, Formulation of a surrogate for the simulation of jet fuel pool fires, Combust. Sci. Technol. 177 (2005) 715–739.

[8] H. Richter, J.B. Howard, Formation of polycyclic aromatic hydrocarbons and their growth to soot—a review of chemical reaction pathways, Prog. Energy Combust. Sci. 26 (4–6) (2000) 565–608.

[9] A. D'Anna, Combustion-formed nanoparticles, Proc. Combust. Inst. 32 (1) (2009) 593–613.

[10] K. Brezinsky, The high-temperature oxidation of aromatic hydrocarbons, Prog. Energy Combust. Sci. 12 (1) (1986) 1–24.

[11] C.S. McEnally, L.D. Pfefferle, B. Atakan, K. Kohse-Höinghaus, Studies of aromatic hydrocarbon formation mechanisms in flames: progress towards closing the fuel gap„ Prog. Energy Combust. Sci. 32 (2006) 247–294.

[12] J.D. Bittner, J.B. Howard, Composition profiles and reaction mechanisms in a near-sooting premixed benzene/oxygen/argon flame, Proc. Combust. Inst. 18 (1) (1981) 1105–1116.

[13] A. Tregrossi, A. Ciajolo, R. Barbella, The combustion of benzene in rich premixed flames at atmospheric pressure, Combust. Flame 117 (3) (1999) 553–561.

[14] M. Sirignano, M. Alfè, A. Tregrossi, A. Ciajolo, A. D'Anna, Experimental and modeling study on the molecular weight distribution and properties of carbon particles in premixed sooting flames, Proc. Combust. Inst. 33 (1) (2011) 633–640.

[15] A. D'Anna, M. Commodo, P. Minutolo, Particle inception in a laminar premixed flame of benzene, Combust. Sci. Technol. 180 (5) (2008) 758–766.

[16] C. Russo, F. Stanzione, A. Tregrossi, M. Alfè, A. Ciajolo, The effect of temperature on the condensed phases formed in fuel-rich premixed benzene flames, Combust. Flame 159 (7) (2012) 2233–2242.

[17] C. Russo, M. Alfè, J.-N. Rouzaud, F. Stanzione, A. Tregrossi, A. Ciajolo, Probing structures of soot formed in premixed flames of methane, ethylene and benzene, Proc. Combust. Inst. 34 (2013) 1885–1892.

[18] M. Alfè, B. Apicella, R. Barbella, J.N. Rouzaud, A. Tregrossi, A. Ciajolo, Structure–property relationship in nanostructures of young and mature soot in premixed flames, Proc. Combust. Inst. 32 (1) (2009) 697–704.

[19] B. Apicella, P. Pré, M. Alfè, A. Ciajolo, V. Gargiulo, C. Russo, TregrossiA. C., D. Deldique, J.N. Rouzaud, Soot nanostructure evolution in premixed flames by high resolution electron transmission microscopy (HRTEM), Proc. Combust. Inst. 35 (2) (2015) 1895–1902.

[20] C.A. Echavarria, A.F. Sarofim, J.S. Lighty, A. D'Anna, Modeling and measurements of size distributions in premixed ethylene and benzene flames, Proc. Combust. Inst. 32 (1) (2009) 705–711.

[21] A.D. Abid, E.D. Tolmachoff, D.J. Phares, H. Wang, Y. Liu, A. Laskin, Size distribution and morphology of nascent soot in premixed ethylene flames with and without benzene doping, Proc. Combust. Inst. 32 (1) (2009) 681–688.

[22] C.S. McEnally, L.D. Pfefferle, Improved sooting tendency measurements for aromatic hydrocarbons and their implications for naphthalene formation pathways, Combust. Flame 148 (4) (2007) 210–222.
[23] M. Conturso, M. Sirignano, A. D'Anna, Effect of alkylated aromatics on particle formation in diffusion flames: an experimental study,, Exp. Thermal Fluid Sci. 73 (2016) 27–32.
[24] T. Zhang, L. Zhao, M.J. Thomson, Effects of n-propylbenzene addition to n-dodecane on soot formation and aggregate structure in a laminar coflow diffusion flame, Proc. Combust. Inst. 36 (1) (2017) 1339–1347.
[25] C. Russo, L. Giarracca, F. Stanzione, B. Apicella, A. Tregrossi, A. Ciajolo, Sooting structure of a premixed toluene-doped methane flame, Combust. Flame 190 (2018) 252–259.
[26] C. Russo, A. D'Anna, A. Ciajolo, M. Sirignano, Modelling analysis of PAH and soot measured in a premixed toluene-doped methane flame, Fuel 234 (2018) 1026–1032.
[27] A. D'Anna, M. Alfè, B. Apicella, A. Tregrossi, A. Ciajolo, Effect of fuel/air ratio and aromaticity on sooting behavior of premixed heptane flames, Energy Fuels 21 (5) (2007) 2655–2662.
[28] Q. Tang, B. Ge, Q. Ni, B. Nie, X. You, Soot formation characteristics of n-heptane/toluene mixtures in laminar premixed burner-stabilized stagnation flames, Combust. Flame 187 (2018) 239–246.
[29] M.L. Botero, S. Mosbach, M. Kraft, Sooting tendency and particle size distributions of n-heptane/toluene mixtures burned in a wick-fed diffusion flame, Fuel 169 (2016) 111–119.
[30] H. Richter, S. Granata, W.H. Green, J.B. Howard, Detailed modeling of PAH and soot formation in a laminar premixed benzene/oxygen/argon low-pressure flame, Proc. Combust. Inst. 30 (2005) 1397–1405.
[31] J.Y. Hwang, W. Lee, G. Kang, S.H. Chung, Synergistic effect of ethylene–propane mixture on soot formation in laminar diffusion flames, Combust. Flame 114 (1998) 370–380.
[32] S.M. Lee, S.S. Yoon, S.H. Chung, Synergistic effect on soot formation in counterflow diffusion flames of ethylene–propane mixtures with benzene addition, Combust. Flame 136 (2004) 493–500.
[33] S. Trottier, H. Guo, G.J. Smallwood, M.R Johnson, Measurement and modeling of the sooting propensity of binary fuel mixtures, Proc. Combust. Inst. 31 (1) (2007) 611–619.
[34] A.D. Eisner, D.E. Rosner, Experimental studies of soot particle thermophoresis in nonisothermal combustion gases using thermocouple response techniques, Combust. Flame 61 (2) (1985) 153–166.
[35] M. Salamanca, M. Sirignano, A D'Anna, Particulate formation in premixed and counter-flow diffusion ethylene/ethanol flames, Energy Fuels 26 (2012) 6144–6152.
[36] M. Sirignano, M. Salamanca, A. D'Anna, The role of dimethyl ether as substituent to ethylene on particulate formation in premixed and counter-flow diffusion flames, Fuel 126 (2014) 256–262.
[37] M. Conturso, M. Sirignano, A. D'Anna, Effect of furanic biofuels on particles formation in premixed ethylene–air flames: an experimental study, Fuel 175 (2016) 137–145.
[38] M. Sirignano, D. Bartos, M. Conturso, M. Dunn, A. D'Anna, A.R. Masri, Detection of nanostructures and soot in laminar premixed flames, Combust. Flame 176 (2017) 299–308.
[39] H. Bladh, N.E. Olofsson, T. Mouton, J. Simonsson, X. Mercier, A. Faccinetto, P.E. Bengtsson, P. Desgroux, Probing the smallest soot particles in low-sooting premixed flames using laser-induced incandescence, Proc. Combust. Inst. 35 (2) (2015) 1843–1850.
[40] H.A. Michelsen, Probing soot formation, chemical and physical evolution, and oxidation: a review of in situ diagnostic techniques and needs, Proc. Combust. Inst. 36 (1) (2017) 717–735.
[41] P. Desgroux, A. Faccinetto, X. Mercier, T. Mouton, D.A. Karkar, A. El Bakali, Comparative study of the soot formation process in a "nucleation" and a "sooting" low pressure premixed methane flame, Combust. Flame 184 (2017) 153–166.
[42] M. Sirignano, A. D'Anna, Coagulation of combustion generated nanoparticles in low and intermediate temperature regimes: an experimental study, Proc. Combust. Inst. 34 (1) (2013) 1877–1884.
[43] M. Conturso, M. Sirignano, A. D'Anna, Effect of 2,5-dimethylfuran doping on particle size distributions measured in premixed ethylene/air flames, Proc. Combust. Inst. 36 (2017) 985–992.
[44] C. Russo, A. D'Anna, A. Ciajolo, M. Sirignano, The effect of butanol isomers on the formation of carbon particulate matter in fuel-rich premixed ethylene flames, Combust, Flame 199 (2019) 122–130.
[45] G.P. Reischl, J.M. Mäkelä, R. Karch, J. Neeid, Bipolar charging of ultrafine particles in the size range below 10 nm, J. Aerosol Sci. 27 (1996) 931–949.
[46] P. Minutolo, A. D'Anna, A. D'Alessio, On detection of nanoparticles below the sooting threshold, Combust. Flame 152 (2008) 287–292.
[47] L.A. Sgro, A. D'Anna, P. Minutolo, Charge distribution of incipient flame-generated particles, Aerosol. Sci. Technol. 44 (2010) 651–662.
[48] W.C. Hinds, Aerosol Technology: Properties, Behavior and Measurement of Airborne Particles, Wiley, New York (1982), p. 163
[49] J. Singh, R.I. Patterson, M. Kraft, H. Wang, Numerical simulation and sensitivity analysis of detailed soot particle size distribution in laminar premixed ethylene flames, Combust. Flame 145 (1–2) (2006) 117–127.
[50] M. Sirignano, J. Kent, A. D'Anna, Modeling formation and oxidation of soot in nonpremixed flames, Energy Fuels 27 (4) (2013) 2303–2315.
[51] M. Sirignano, J. Kent, A. D'Anna, Further experimental and modelling evidences of soot fragmentation in flames, Proc. Combust. Inst. 35 (2) (2015) 1779–1786.
[52] M. Sirignano, J. Kent, A. D'Anna, Detailed modeling of size distribution functions and hydrogen content in combustion-formed particles, Combust. Flame 157 (6) (2010) 1211–1219.
[53] A. D'Anna, M. Sirignano, J. Kent, A model of particle nucleation in premixed ethylene flames, Combust. Flame 157 (11) (2010) 2106–2115.
[54] N.A. Eaves, S.B. Dworkin, M.J. Thomson, Assessing relative contributions of PAHs to soot mass by reversible heterogeneous nucleation and condensation, Proc. Combust. Inst. 36 (1) (2017) 935–945.
[55] J. Israelachvili, Intermolecular and surface forces Academic Press, London (UK) (1991).
[56] A. D'Alessio, A.C. Barone, R. Cau, A. D'Anna, P. Minutolo, Surface deposition and coagulation efficiency of combustion generated nanoparticles in the size range from 1 to 10 nm, Proc. Combust. Inst. 30 (2) (2005) 2595–2603.